Structural Basis for Differences in Substrate Selectivity in Kex2 and Furin Protein Convertases[†,‡]

Todd Holyoak,[§] Charles A. Kettner,[||] Gregory A. Petsko,[§] Robert S. Fuller,[⊥] and Dagmar Ringe*[,§]

Rosenstiel Basic Medical Sciences Research Center, Brandeis University, Waltham, Massachusetts 02454, Dupont Pharmaceuticals Company, Wilmington, Delaware 19880, and Department of Biological Chemistry, University of Michigan Medical School, Ann Arbor, Michigan 48109

Received October 14, 2003; Revised Manuscript Received December 23, 2003

ABSTRACT: Kex2 is the yeast prototype of a large family of serine proteases that are highly specific for cleavage of their peptide substrates C-terminal to paired basic sites. This paper reports the 2.2 Å resolution crystal structure of ssKex2 in complex with an Ac-Arg-Glu-Lys-Arg peptidyl boronic acid inhibitor ($R = 19.7$, $R_{free} = 23.4$). By comparison of this structure with the structure of the mammalian homologue furin [Henrich, S., et al. (2003) *Nat. Struct. Biol. 10*, 520−526], we suggest a structural basis for the differences in substrate recognition at the P_2 and P_4 positions between Kex2 and furin and provide a structural rationale for the lack of P_6 recognition in Kex2. In addition, several monovalent cation binding sites are identified, and a mechanism of activation of Kex2 by potassium ion is proposed.

In *Saccharomyces cerevisiae*, Kex2 (kexin, EC 3.4.21.61), a Ca^{2+}-dependent transmembrane protease, is necessary for production and secretion of mature α-factor and killer toxin by proteolysis at paired basic sites (*2*−*5*). Pleiotropic effects of deleting the *KEX2* gene suggest the existence of additional targets (*6*, *7*) that likely induce cell wall proteins and enzymes (*8*, *9*). The Kex2 homologues in pathogenic fungi *Candida albicans* and *Candida glabrata* are virulence factors (*10*, *11*) with the *C. albicans* molecule implicated in the processing of at least 33 additional proteins in *C. albicans* (*10*). Mammalian members of the Kex2 family of protein convertases include furin, PC2, PC3/PC1, PC4, PACE4, PC5/6, and PC7/LPC (*12*). In mammals, the protein convertases have been demonstrated to be required for processing of virtually all neuropeptides and peptide hormones as well as proinsulin, coagulation factors, and many growth factors and their receptors (*13*). In addition, furin has been shown to process cancer-associated extracellular metallomatrix proteases and Alzheimer-related secretases and be necessary for the activation of bacterial toxins such as diphtheria and anthrax toxins (*14*). Together, the protein convertases comprise a discrete branch of the subtilase superfamily spanning eukaryotes from yeast to humans (*15*). The protein convertases are distinct from the other members of the subtilase family in that the protein convertase family is highly selective for cleavage of substrates containing paired basic sites, most often KR or RR, unlike the rather nonspecific degradative subtilases. Members of the family share a common domain architecture consisting of a propeptide, which is intramolecularly cleaved (*16*, *17*), a subtilisin-like catalytic domain, a middle domain termed either the homoB- or P-domain (*18*, *19*), and a carboxy-terminal domain. While the catalytic and P-domains display reasonable levels of similarity between the family members, the pro-domains and carboxy-terminal domains have little similarity.

Very little was known about the structural basis for the selectivity of these enzymes prior to the availability of the recently determined crystal structures of Kex2 (*20*) and furin (*21*). The primary sequences of the two enzymes are 38% identical in the sequences of the catalytic and P-domains, and a comparison of the two structures reveals that the two enzymes are structurally quite similar with a C_α rmsd of 1.4 Å with the catalytic residues and those residues involved in P1 recognition and active site Ca^{2+} binding completely conserved (Table 1).[1] In contrast to the structural similarities, kinetic experiments have shown considerable differences in substrate selectivities between the two enzymes. Biochemical characterization of Kex2 has shown that most of its selectivity arises through interactions at P_1 and P_2 (*22*−*24*). Furin, however, seems to generate most of its selectivity through interactions with both P_1 and P_4, with interactions at P_2 being less important (*22*, *24*, *25*). Data also suggest that extended contacts with P_6 are present in furin between the enzyme and substrates (*25*, *26*). This difference between Kex2 and furin specificity determinants seems to define two discrete subsets within the eukaryotic family of processing proteases. It is therefore of great interest to determine how two enzymes of such structural similarity can have such different catalytic properties.

[†] This work was supported in part by NIH Grant GM39697 (to R.S.F.) and by a supplement to that grant (to D.R.) and in part by a grant from the Lucille P. Markey Charitable Trust to Brandeis University.

[‡] Coordinates and structure factors have been deposited in the RCSB Protein Data Bank as entry 1R64.

* To whom correspondence should be addressed. E-mail: ringe@brandeis.edu.

[§] Brandeis University.

[||] Retired from Dupont Pharmaceuticals Co.

[⊥] University of Michigan Medical School.

[1] The designation of the cleavage sites follows the naming convention of Schechter and Berger (*1*) in which the cleavage site lies between P_1 and P_1' with the C-terminus lying on the prime side.

10.1021/bi035849h CCC: $27.50
Published on Web 02/10/2004

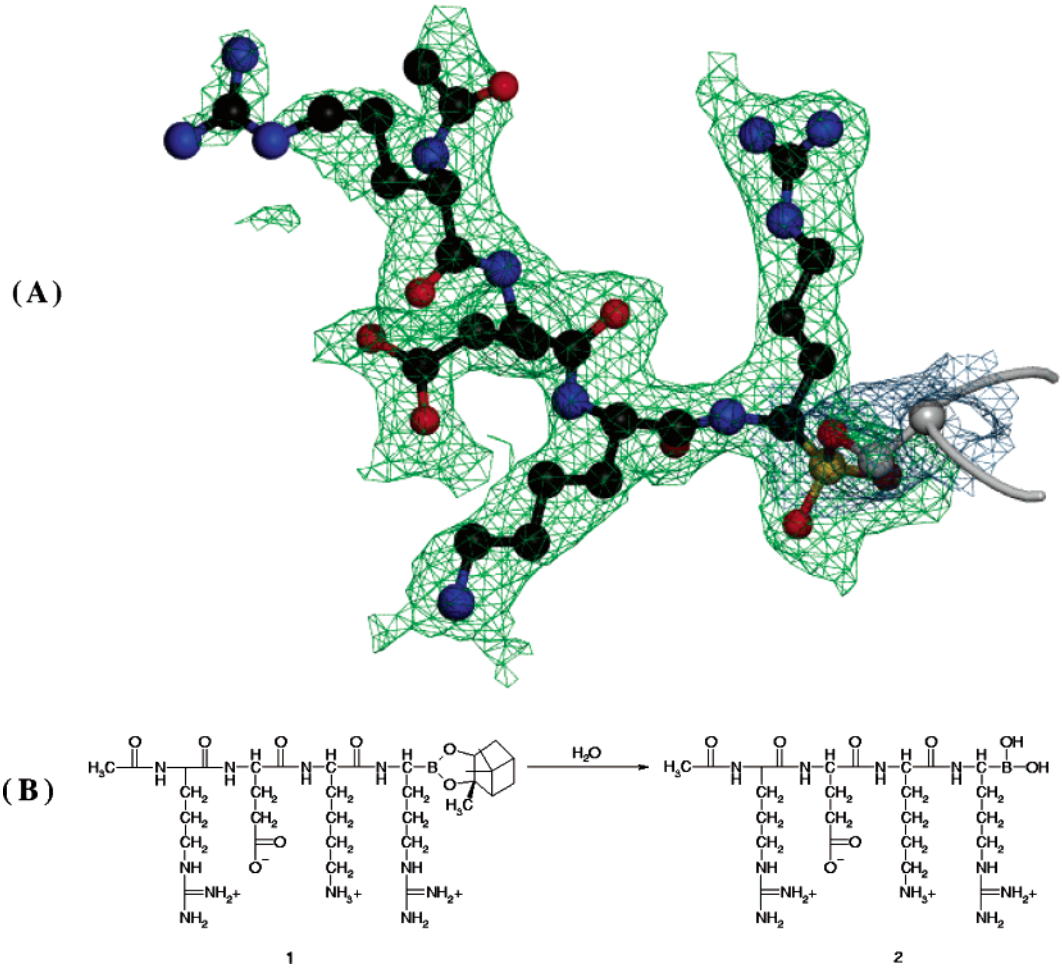

FIGURE 1: Ac-Arg-Glu-Lys-boroArg inhibitor of ssKex2. (A) Electron density maps with $2F_o - F_c$ and $F_o - F_c$ coefficients for the bound boronic acid inhibitor and S385 prior to inclusion of the inhibitor in the model. The final model of the inhibitor has been superimposed. Shown in blue is the difference electron density map with $2F_o - F_c$ coefficients rendered at 1σ and in green with $F_o - F_c$ coefficients at 2σ. The carbon atoms of the inhibitor are shown in black, while the enzyme carbon atoms are rendered in gray. (B) Line drawing representation of Ac-Arg-Glu-Lys-boroArg-pinanediol inhibitor **1**, which upon addition to an aqueous solvent becomes the active boronic acid species **2**. All figures were generated using POVscript+ (http://www.brandeis.edu/~fenn/povscript) (*38*) and rendered using POVRay (http://www.povray.org).

Table 1: Catalytic, S_1, S_2, and S_4 Residues of Kex2 and Furin

site	Kex2	furin	site	Kex2	furin
catalytic	D175	D153	S_2	D175	D153
	H213	H194		D176	D154[c]
	S385	S368		D210[d]	D191[d]
S_1[a]	D276	D257		D211	N192[c]
	D277	D258	S_4	I250[b]	–
	A311[b]	A292[b]		E255	E236
	D320	D301		–	D264
	D325	D306		–	Y308
	E350	E331			

[a] Those residues interacting with both the P_1 side chain and the catalytic calcium ion are indicated. [b] Backbone carbonyl. [c] At S_2, only D154 and N192 interact with the P_2 lysine side chain; D191, while conserved, is oriented away from the P_2 lysine. [d] While not directly interacting with the P_2 side chain, D210 (D191 in furin) provides additional localized negative charge at the S_2 subsite.

This paper reports the crystal structure at 2.2 Å resolution of ssKex2[2] in complex with a P_4-containing peptidyl boronic acid inhibitor (boro-P4). This work demonstrates the structural basis for the differences in P_2 and P_4 selectivity between Kex2 and furin and provides a structural rationale for the lack of P_6 recognition in Kex2. In addition, several monovalent cation binding sites are revealed that provide insight into the mechanism by which Kex2 is activated and, at higher concentrations, inhibited by potassium ions (*27*).

[2] Abbreviations: boro-P3, Ac-Ala-Lys-boroArg peptidyl boronic acid inhibitor; boro-P4, Ac-Arg-Glu-Lys-boroArg peptidyl boronic acid inhibitor; CMK, chloromethyl ketone; DMSO, dimethyl sulfoxide; Glc-Nac, *N*-acetylglucosamine; NCS, noncrystallographic symmetry; ssKex2, secreted soluble Kex2.

EXPERIMENTAL PROCEDURES

Materials. Bis-Tris buffer was purchased from Research Organics (Cleveland, OH). The substrate Boc-Gln-Arg-Arg-AMC was purchased from Bachem. The boronic acid inhibitor, Ac-Arg-Glu-Lys-boroArg-pinanediol (**1**) (Figure 1B), was synthesized by methods described previously (*28*).

Crystallographic materials and screening kits were purchased from Hampton Research (Laguna Nuguel, CA). Malonic acid was purchased from Sigma (St. Louis, MO), and a saturated solution at pH 7.2 was prepared as previously described (*29*) with the exception that the solution was titrated with KOH. All other reagents were of the highest available purity.

Kex2 Expression and Purification. The Kex2 protein concentration was determined using a calculated extinction

coefficient ϵ_{280} of 0.595 mL/mg (*30*; http://us.expasy.org/sprot/). This value was found to compare well with that determined using the Bio-Rad and Pierce colorimetric methods.

Secreted soluble Kex2 (ssKex2) was prepared as previously described (*20*). Following purification, Kex2 was inactivated using a 4-fold molar excess of the inhibitor Ac-Arg-Glu-Lys-boroArg (boro-P4) dissolved in DMSO. The inactivation mix was incubated overnight at 4 °C, and was subsequently assayed to ensure no enzyme activity remained. The protein solution was concentrated to a final volume of 1.5−2.0 mL and loaded onto an S-100 gel filtration column (Pharmacia, Piscataway, NJ), equilibrated in 40 mM Bis-Tris (pH 7.2), 10 mM NaCl, 2 mM $CaCl_2$ buffer. Fractions containing protein were run on SDS−PAGE, and only those fractions containing a band corresponding to full-length ssKex2 were retained. The fractions were pooled, concentrated to 25 mg/mL, and stored at 4 °C.

Crystallization. ssKex2 (25 mg/mL), in 40 mM Bis-Tris (pH 7.2), 10 mM NaCl, and 2 mM $CaCl_2$, was crystallized by the hanging drop method against 2.1 M NH_4SO_4 and 3% DMSO at 25 °C. Crystals grew over a period of 2−4 weeks from 6 μL drops containing 4 μL of protein solution and 2 μL of well solution. Crystals of ssKex2 were transferred from the growth drop into a depression plate containing a 10 μL drop of 50% saturated potassium malonate (pH 7.2). The crystals were allowed to equilibrate for a period of several minutes and then cryocooled in liquid nitrogen (*31*).

Data Collection. Data were collected on cryocooled crystals maintained at 100 K throughout data collection at the Advanced Photon Source (APS) Biocars 14-ID-B beamline using an ADSC Quantum-4 CCD detector. All data were integrated and scaled with DENZO and SCALEPACK, respectively (*32*). See Table 2 for data statistics.

Structure Determination and Refinement. The crystals of the boro-P4-inhibited enzyme were isomorphous with the crystals used for the 2.4 Å resolution crystal structure of the boro-P3-inhibited enzyme [PDB entry 1OT5 (*20*)]; therefore, this model was used as a starting point for the current structure. All calcium ions and water, sugar, and inhibitor molecules were removed from the model prior to an initial round of rigid body refinement using the program CNS (*33*). The initial model was then subjected to a round of simulated annealing torsion angle refinement in CNS (*34*) followed by manual model adjustment with the modeling program O, coordinate minimization, and individual *B*-factor refinement. All data were refined (no σ cutoff was utilized) with a test set of 10% of the data set aside for use in calculation of R_{free} (*35*). Bulk solvent correction and anisotropic scale factors were applied to the data. Throughout the refinement, extremely tight NCS restraints were applied (excluding residues 125, 139, 212, 225, 253, 265, 317, 378, 428, 437, 461, 473−476, 484, 488−490, 494, 496, 498, 518, 533, and 903−906), as tests with lower NCS restraint weights did not result in a significant improvement in the R_{free} value (*35*). A total of 756 waters, six Ca^{2+} atoms, six K^+ atoms, seven sugars, and one Bis-Tris molecule were added to the model near the end of refinement, in addition to the peptidyl boronic acid inhibitor. The final model refined to an *R*-factor of 19.7% (R_{free} = 23.4% for a test set, 10%, of randomly chosen reflections). See Table 2 for final model statistics.

Table 2: Data and Model Statistics for the 2.2 Å Resolution Crystal Structure of Boro-P4-Inhibited ssKex2

beamline	APS-Biocars 14-BMC
wavelength (Å)	0.9
space group	$P6_522$
unit cell (Å)	$a = b = 113.5$, $c = 365.0$
resolution limits	50.0−2.2
no. of unique reflections	59902
completeness[a] (%) (all data)	89.2 (69.5)
redundancy[a]	5.9
$I/\sigma_{(I)}$[a]	22.9 (2.7)
R_{merge}[a,b]	0.05 (0.27)
no. of molecules in the asymmetric unit	2
solvent content (%)	62
no. of amino acid residues	962
no. of water molecules	756
no. of calcium ions	6
no. of potassium ions	6
no. of carbohydrate residues (Glc-Nac)	7
R_{free}[c] (%)	23.4
R_{work}[d] (%)	19.7
average *B*-factor	27.1
Luzzati coordinate error (Å)	0.24
rmsd for bond lengths (Å)	0.01
rmsd for bond angles (deg)	1.20

[a] Values in parentheses represent statistics for data in the highest-resolution shells. The highest-resolution shell comprises data in the range of 2.3−2.2 Å. [b] $R_{merge} = \sum_{hkl}\sum_i|I^i_{hkl} - \langle I_{hkl}\rangle|/\sum_{hkl}\sum_i I^i_{hkl}$, where *i* is the *i*th observation of a reflection with index *hkl* and the broken brackets indicate an average over all *i* observations. [c] R_{free} was calculated as R_{work}, where F^O_{hkl} values were taken from a set of 6042 reflections (10% of the data) that were not included in the refinement (*35*). [d] $R_{work} = \sum_{hkl}|F^C_{hkl} - F^O_{hkl}|/\sum_{hkl}F^O_{hkl}$, where F^C_{hkl} is the magnitude of the calculated structure factor with index *hkl* and F^O_{hkl} is the magnitude of the observed structure factor with index *hkl*.

RESULTS

The 2.2 Å resolution crystal structure of ssKex2 in complex with the Ac-Arg-Glu-Lys-boroArg (boro-P4) inhibitor (Figure 2) is nearly identical to that of the previously determined ssKex2 structure at 2.4 Å resolution (PDB entry 1OT5; C_α rmsd = 0.4 Å) (*20*), which also contains two molecules in the asymmetric unit. The refined model has good stereochemistry: 86.4, 13.2, and 0.4% of the main chain ϕ and ψ angles are in the core, allowed regions, and generously allowed regions, respectively, as calculated using PROCHECK (*36*). No changes between the two structures are observed for any of the amino acid side chains corresponding to the catalytic residues or for residues involved in P_1-P_4 interactions. Whereas the loop composed of residues 198−203 was poorly defined in the 2.4 Å resolution structure, the slightly higher resolution of this structure allowed for minor repositioning of the loop to fit the electron density better. In addition, the higher resolution of the current structure allowed for modeling of two additional residues at the N- and C-termini such that the model now contains residues 121−601. Unexpectedly, density consistent with an additional N-linked glycan at the third consensus asparagine glycosylation sequence (N404) was observed in molecule A of the crystallographic dimer in the asymmetric unit and was included in the model. In the current structure, the crystals were cryocooled in potassium malonate, in contrast to the sodium malonate solution used in the previously reported structure of Kex2 (*20*). Three potassium binding sites per monomer were identified on the basis of their low *B*-factors when modeled as water molecules and their modest

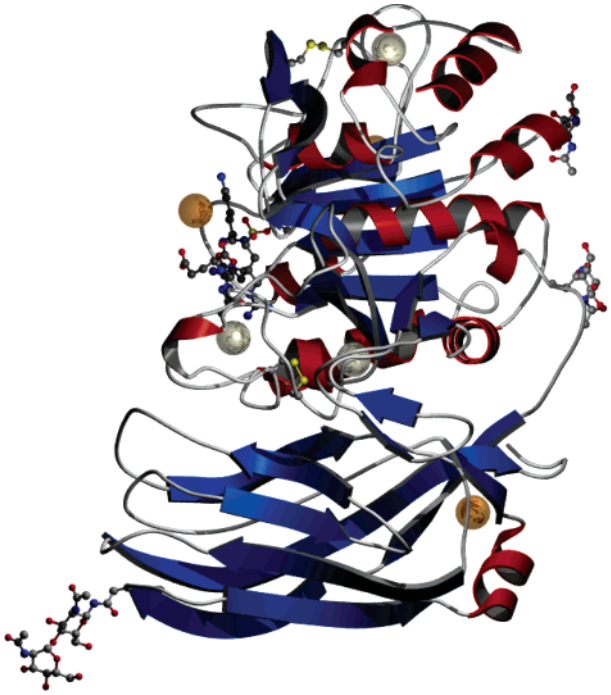

FIGURE 2: Ribbon diagram of the monomer of ssKex2. The GlcNac residues, disulfide bonds, catalytic triad, and inhibitor are shown as ball-and-stick representations. The calcium and potassium ions are rendered as white and copper spheres, respectively.

anomalous signal at the wavelength at which the data were collected, the latter of which would rule out the possibility of the atoms being nitrogen or oxygen. As shown in Figure 2, potassium atoms are bound near both the N- and C-termini of the molecule. These two sites have symmetry-related sites in the second molecule in the asymmetric unit (data not shown). Each molecule in the asymmetric unit also contains a third K^+ ion binding site that is unique to each molecule in the asymmetric unit. In the case of the A molecule (Figure 2), this potassium is bound near the active site and its binding site is partly formed through second sphere coordination by the P_3 glutamate side chain of the inhibitor and E422 from molecule B in the crystallographic dimer. The third K^+ ion bound in the B molecule is situated in a well-hydrated pocket between the catalytic and P-domains near H345 and R444.

Electron density consistent with a molecule of Bis-Tris buffer was observed at the active site forming a direct interaction with R542 through two of the hydroxyl groups of the buffer molecule. Previous studies have shown that Bis-Tris buffer is a particularly stabilizing buffer for Kex2 when compared to other biological buffers (*37*). Electron density suggestive of additional Bis-Tris molecules was also observed, but the quality of the electron density was not suitable for inclusion of these molecules in the final model. Finally, R542 from the P-domain occupies a rotomer different from that observed for the same amino acid in the boro-P3-inhibited structure. In this instance, the side chain is oriented to make contacts with the B molecule in the crystallographic dimer rather than forming a hydrogen bond with the backbone carbonyl of D278 as previously observed.

As shown in Figure 3A, the boro-P4 inhibitor is bound to ssKex2 in a fashion identical to that previously observed for the shorter inhibitor (*20*), with the N-terminal acetyl group of the boro-P3 inhibitor aligning with the carbonyl of the arginine at P_4 in the boro-P4 inhibitor.

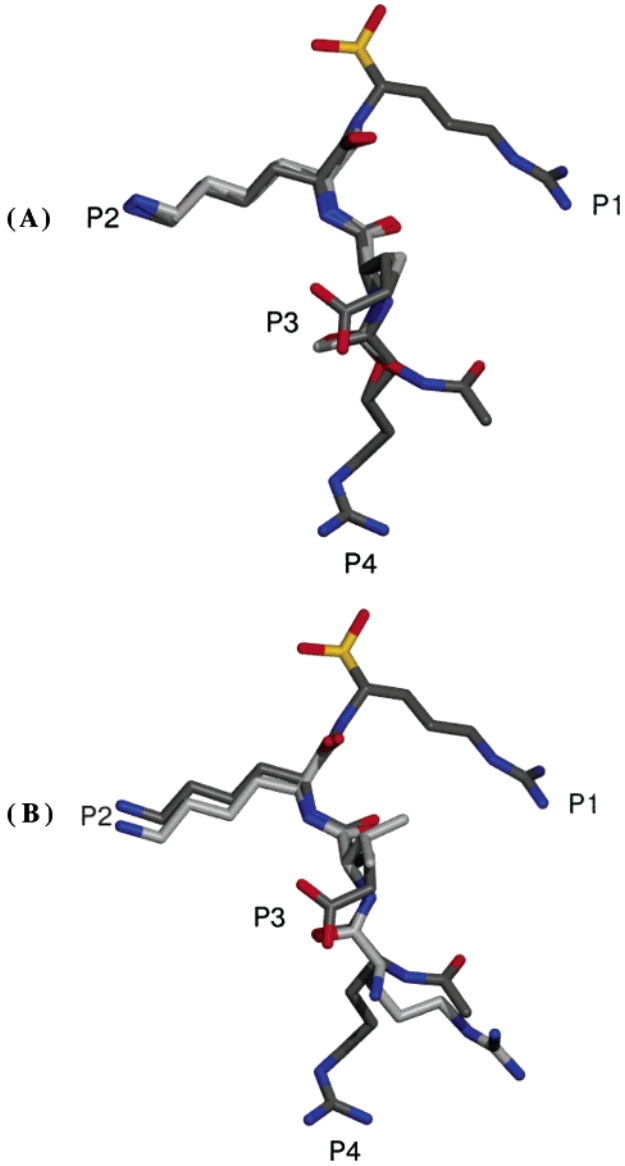

FIGURE 3: Superpositioning of (A) boro-P3 (PDB entry 1OT5) and boro-P4 peptidyl boronic acids bound to ssKex2 and (B) boro-P4 peptidyl boronic acid bound to ssKex2 and dec-RVKR-CMK bound to furin (PDB entry 1P8J). Carbon atoms of the boro-P4 inhibitor are rendered in black, while the carbon atoms of the boro-P3 boronic acid and the CMK bound to furin are rendered in gray. The boron is rendered in gold, and all other atoms are colored by atom type.

The current structure allows for identification of the S_4 binding pocket of Kex2 (Figures 4 and 5). The P_4 arginine side chain of the inhibitor is coordinated by the carboxylate of E255 and the backbone carbonyl of I250. The electron density for the P_4 arginine is poorer in quality than that observed for the other residues of the inhibitor (Figure 1) and has the highest thermal factors ($\sim$40 Å^2) of any of the inhibitor residues. A hydrophobic pocket at S_4 is also present and is composed of residues I245, L246, I250, and W273 (Figure 5). All of the amino acid residues forming the P_4 binding site are situated in positions identical to their positions in the previous boro-P3−Kex2 structure, indicating that occupancy of this site does not induce a conformational change (data not shown).

DISCUSSION

The structure of Kex2 in complex with the peptidyl boronic acid, Ac-Ala-Lys-borArg (*20*), explained the structural basis

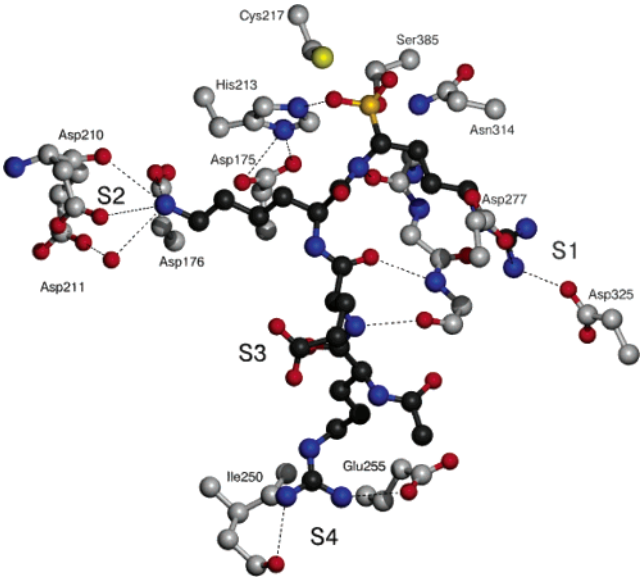

FIGURE 4: Overall view of the ssKex2 subsite architecture illustrating the arrangement of the S_1-S_4 subsites. Those amino acids making contacts with the inhibitor are shown. The atoms are colored according to atom type, and the boron atom is rendered in gold. The catalytic triad of D175, H213, and S385, the oxyanion hole N314, and the reactive C217 are also shown.

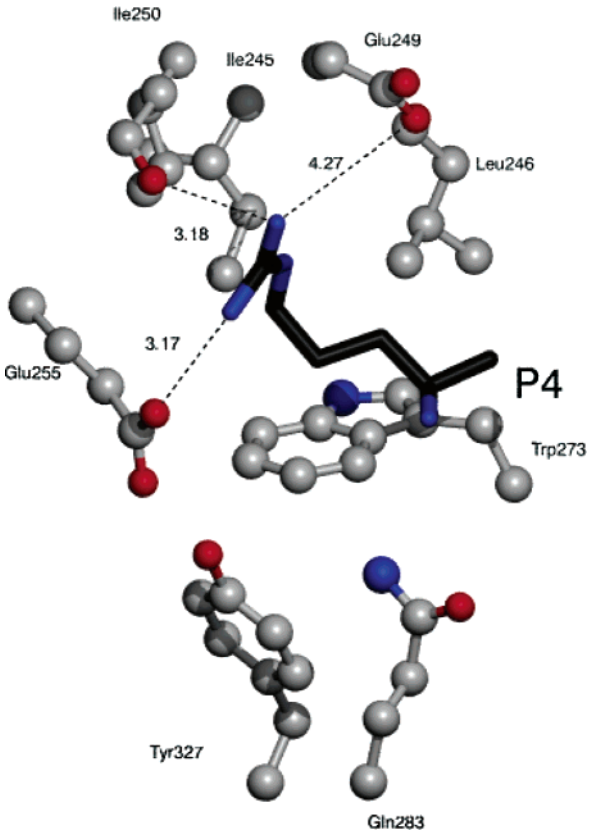

FIGURE 5: ssKex2 S_4 binding pocket. Those residues comprising the S_4 binding site are shown, and the distances to the P_4 side chain of the peptidyl boronic acid inhibitor are indicated. The protein carbon atoms are rendered in gray, while the inhibitor carbon atoms are rendered in black. All other atoms are colored by atom type.

for the selectivity of Kex2 for its prototypical KR cleavage motif. With the recent determination of the structure of furin, the mammalian homologue of Kex2, the question of how these two similar structures have evolved to achieve different selectivities for their protein substrates can be addressed.

A comparison of the sequences and structures of Kex2 and furin shows that the sequences of the two enzymes are 38% identical in the sequences of the catalytic and P-domains and have a C_α rmsd of 1.4 Å over this same region, demonstrating the striking similarity of these two enzymes. Despite a high degree of structural similarity, Kex2 and furin differ in their substrate selectivity in kinetic experiments. Whereas Kex2 generates most of its selectivity through interactions with P_1 and P_2 and has a dual specificity for basic and branched chain aliphatic amino acids at P_4 (*22*−*24*), furin has a reduced level of selectivity at P_2 and relies more heavily on interactions at P_1 and P_4 (*22*, *24*, *25*). In addition, furin has been shown to have extended interactions with longer sequences out to P_6 which have been suggested to be unimportant in the hydrolysis of substrates by Kex2 (*24*, *25*). Unfortunately, these differences in selectivity cannot be addressed with the previously determined structure of Kex2 because this structure did not contain a P_4 residue in the bound inhibitor, whereas the structure of furin in complex with a tetrapeptidyl chloromethyl ketone did. The current 2.2 Å resolution crystal structure of Kex2 in complex with a longer peptidyl boronic acid inhibitor contains an arginine residue at P_4 (Figures 1 and 2) and thus allows us to address this question through comparison of this structure with that of the structure of furin in complex with decRVKR-CMK [PDB entry1P8J (*21*)].

The current 2.2 Å resolution crystal structure of Kex2 in complex with a longer peptidyl boronic acid (Figures 1 and 2) is quite similar to the previously determined 2.4 Å resolution structure. C_α superpositioning of the two structures results in nearly identical models with the only differences lying in the loop from residue 198 to 203, which is better defined in the higher-resolution structure, resulting in a slight repositioning of the loop in the current model. In addition, R542, which in the previous structure was involved in a hydrogen bond with the backbone carbonyl of D278 that stabilized the active site calcium binding loop, is in a different orientation in the current structure. In the current structure, the occupied rotomer does not form a hydrogen bond with the backbone carbonyl of D278 as seen in the previous structure. This result suggests that this interaction may not be an important stabilizing factor for the active site calcium binding loop as was previously suggested (*20*). Figure 3A shows that the superpositioning of the two structures also results in the boro-P3 and boro-P4 inhibitors aligning very well, with the C-terminal acetyl group of the boro-P3 inhibitor superpositioned upon the carbonyl group of the P_4 arginine in the boro-P4 inhibitor. It is apparent that the S_4 binding pocket is predetermined by the enzyme in the absence of its occupancy because none of the amino acid residues that form the P_4 binding pocket differ in their position from that observed in the boro-P3−Kex2 complex. From the poorer electron density and higher thermal factors for the P_4 arginine side chain, it is also apparent that the P_4 side chain is more disordered than the side chains of the residues at P_1 and P_2. This may be explained by the P_4 arginine being coordinated by only the backbone carbonyl of I250 and the carboxylate of E255 (Figures 4 and 5).

As previously mentioned, Kex2 has a dual specificity for both basic and aliphatic residues at P_4, with all but two of the known Kex2 physiological substrates containing aliphatic residues at this position (*23*). The presence of a discrete

Table 3: Steady-State Kinetic Parameters for Kex2 and Furin P_4 Specificity[a]

substrate	k_{cat}/K_M (M^{-1} s^{-1})	relative k_{cat}/K_M
	Kex2[b]	
Ac***β***YKK↓MCA	9.2×10^4	1.0
AcRYKK↓MCA	1.2×10^5	1.3
AcÇYKK↓MCA	4.9×10^3	0.053
AcAYKK↓MCA	1.2×10^3	0.013
AcDYKK↓MCA	<250	<0.003
AcFYKK↓MCA	3.7×10^4	0.4
AcχYKK↓MCA	1.3×10^5	1.4
	Furin[c]	
AcRARYKR↓**MCA**	2.6×10^6	1.0
AcRAKYKR↓MCA	8.3×10^4	0.032
AcRAAYKR↓MCA	<1000	<0.0004
AcRAπYKR↓MCA	4.4×10^3	0.0017

[a] Ac, acetyl; β, norleucine; Ç, citrulline; π, norvaline; χ, β-cyclohexylalanine; MCA, methylcoumarinamide. [b] Values taken from ref *23*. [c] Values taken from ref *25*.

hydrophobic pocket comprised of residues I245, L246, I250, and W273 would explain the selectivity of Kex2 for aliphatic residues at this position (Figure 5). The modest selection against phenylalanine (2.5-fold, Table 3) at this position can likely be explained by steric constraints imposed by the bulkiness of the phenylalanine ring or by the rigidity imposed by the ring structure compared to the conformational flexibility of the branched chain aliphatics that have been tested (Table 3). The nature of the basic binding site is discussed below.

The presence of three potassium ions bound per molecule in the ASU is interesting because it has been shown previously that Kex2 is activated by K^+ and other monovalent cations (*27*). Of the observed K^+ ions, the most obvious candidate for an allosteric effector would be the K^+ ion bound near the active site and the P_3 glutamate carboxylate. This appears, however, to be an artifact of crystallization, because one of the second sphere ligands is contributed by the second molecule in the crystallographic dimer (E422). In addition, the boro-P4 P_3 glutamate is a second sphere ligand to the K^+. Therefore, it would be expected that in substrates lacking a glutamate at P_3, the potassium site would not be present and no activation would be observed in the kinetic data. This is not supported by the biochemical data that show an activating effect of potassium with substrates that lack acidic residues at P_3 (*27*). Finally, in the previous Kex2 structure, the inhibitor contained an alanine residue at P_3, and examination of that data reveals no evidence for the binding of a monovalent cation at this site. The third potassium site in the B molecule in the crystallographic dimer is also most likely an artifact of crystallization since it has no direct ligands from the enzyme and is typical of well-ordered monovalent cations found on the surfaces of many proteins at high concentrations. The other two potassium ions that are present in both molecules in the dimer are located at the N- and C-termini of the molecule at a distance quite far from the active site (Figure 2). Since furin also exhibits activation and inhibition by potassium ion similar to those exhibited by Kex2 (*27*), it is of interest to compare these two binding sites of Kex2 with furin. While the N-terminal potassium binding site is not conserved in sequence [ligands; backbone carbonyls of A191, E192, and S194 and phenolic oxygen of Y261 (Figure 7)], the general fold is structurally

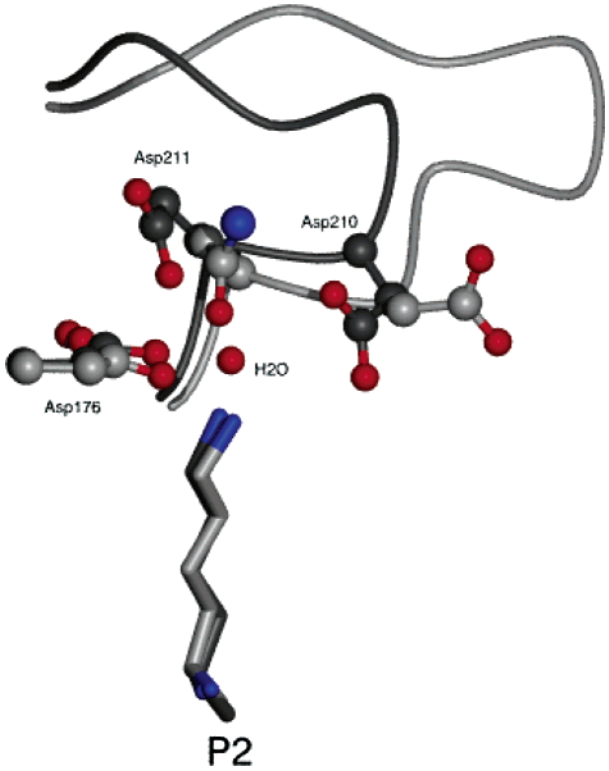

FIGURE 6: S_2 binding pockets of ssKex2 and furin. Superpositioning results of boro-P4 peptidyl boronic acid bound to ssKex2 and dec-RVKR-CMK bound to furin (PDB entry 1P8J) in the region of the S_2 binding site. Carbon atoms of the boro-P4 inhibitor are rendered in black, while the carbon atoms of the CMK bound to furin are rendered in gray. The amino acid side chains of ssKex2 are labeled.

similar in this area between Kex2 and furin (data not shown). However, one of the ligands to the potassium at this site in Kex2 (Y261) is absent in furin (L242, Figure 7), and consequently, this site would be absent in furin. The C-terminal site, with ligands T466 and the backbone carbonyls of W467 and A500, is in a region in which the level of sequence and structural similarity is low, and the site occupied by potassium in Kex2 is occupied by the amide side chain of N479 in furin. These observations would seem to provide evidence that does not support these ions being involved in the kinetic response of Kex2 and furin to potassium and other monovalent cations. In light of the current crystallographic data, we propose an alternative explanation for the observation of activation and inhibition of Kex2 by monovalent cations. In the absence of bound ligand (or product) and in the absence of substantial structural rearrangement, there would be considerable localized negative charge at the S_1 and S_2 subsites. We propose that in the absence of ligand this charge is stabilized by the binding of one or more monovalent species that preorganize and stabilize the subsites; once ligand binds, the cations are displaced and catalysis proceeds. This model provides an explanation for all the observed kinetic phenomena with Kex2 without invoking a discrete allosteric binding site. First, in the presence of potassium, hydrolysis of good substrates is stimulated while hydrolysis of poor substrates is inhibited (*27*). Substrates with good contacts with the subsites would have greater affinity for the enzyme and thus would be able to easily displace the bound cations, while binding of a poorer substrate would be inhibited. Second, at higher concentrations (>1 M), inhibition of catalysis is observed (*27*). As K^+

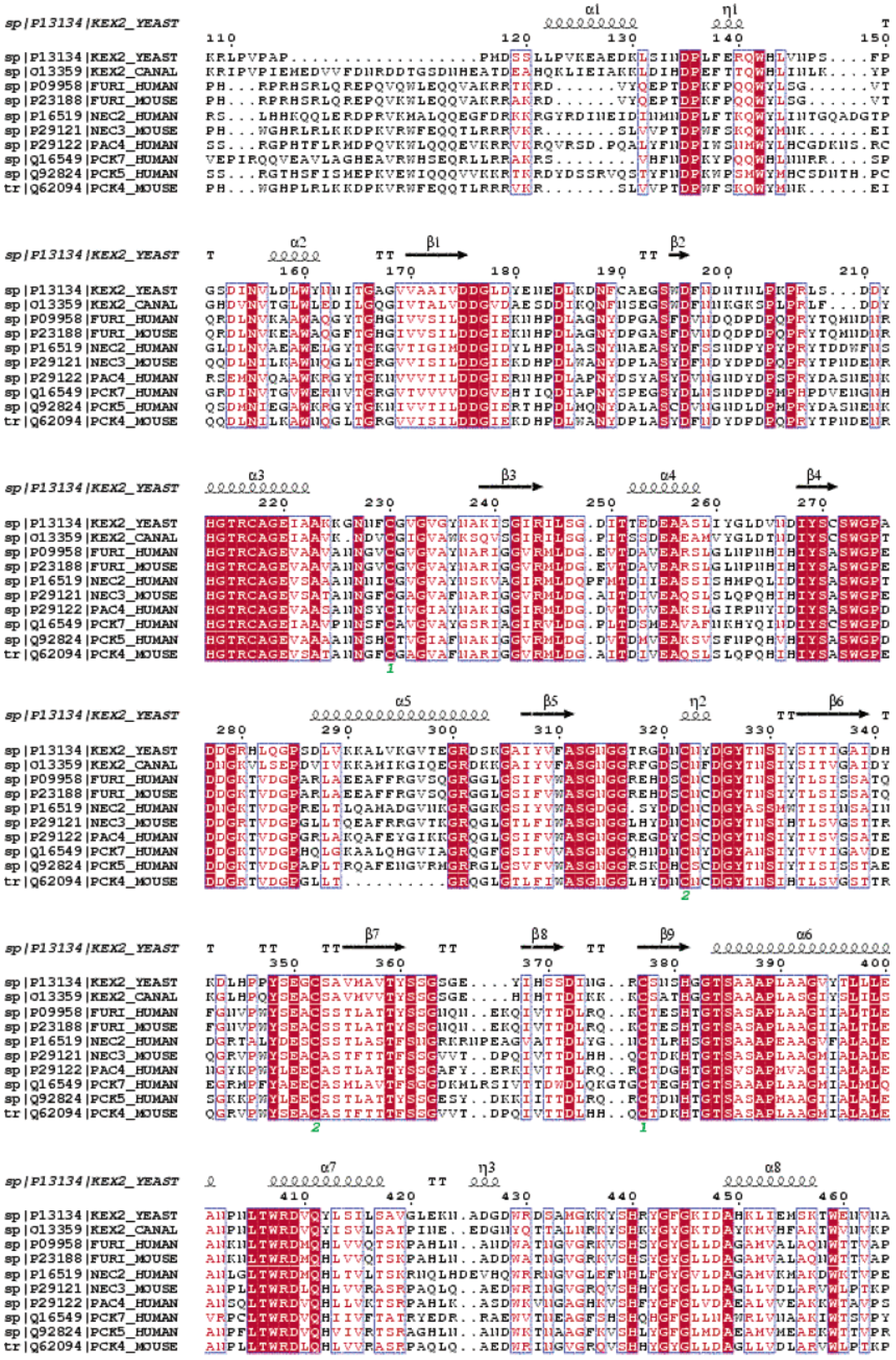

FIGURE 7: Sequence alignment of members of the PC family of processing proteases. The sequences of the enzymes encompassing the mature protease domains (residues 114−457 in Kex2) of *S. cerevisiae* Kex2 (sp|P13134|KEX2_YEAST), *C. albicans* Kex2 (sp|O13359|KEX2_CANAL), human furin (sp|P09958|FURI_HUMAN), mouse furin (sp|*P*23188|FURI_MOUSE), human PC2 (sp|P16519|NEC2_HUMAN), mouse PC3 (sp|P29121|NEC3_MOUSE), human PACE4 (sp|P29122|PAC4_HUMAN), human PC7 (sp|Q16549|PCK7_HUMAN), human PC5 (sp|Q92824|PCK5_HUMAN), and mouse PC4 (tr|Q62094|PCK4_MOUSE) were aligned using Clustal W (*39*) and annotated using ESPript 2.1 (*40*). The annotated secondary structural elements were generated from the structure of Kex2. The numbering of the sequences is based upon the primary sequence of Kex2.

competes with substrate for acidic residues in the binding process, it would be intrinsic to this model that inhibition be observed. At the concentrations of the monovalent cation where inhibition is observed (>1 M), the vast excess of monovalent species would be sufficient to cause an inhibition of binding and overcome the discrepancies in ligand affinity. Finally, potassium ions result in a loss of burst kinetics and therefore slow acylation while accelerating the previously rate-limiting deacylation process, resulting in a more "subtilisin-like" protease (*27*). A slowing of acylation would again be expected in this model since acylation would now include an additional step where the exchange of the bound cation and substrate side chain must occur prior to acylation. Conversely, deacylation would be stimulated by the reverse of the substrate−cation exchange. Because Kex2 is based upon a subtilisin structural scaffold with the predominant structural differences lying in the nature of the substites, and if we note that a similar monovalent cation effect has not been reported in subtilisin, it seems logical that the differences are manifest in those subsites. We feel this simpler model provides a better explanation for the kinetic observations and is supported by the lack of obvious allosteric activators in the currently available Kex2 structures.

The presence of a third N-linked glycosylation site present at N404 is somewhat surprising. Biochemical evidence has previously suggested that Kex2 was glycosylated at only two of the three consensus sites (N163 and N480), a feature also observed in the previously determined structure (*20*). With the higher resolution of the current structure, electron density consistent with N-linked glycosylation at N404 is observed, but only in the A molecule of the crystallographic dimer. This is not too surprising because the A molecule has lower thermal factors than the B molecule, most likely due to crystal packing, and disorder probably results in the glycosyl chain at of N404 in the B molecule not being observed.

Interactions between the P_1 and P_2 side chains of the boro-P4 inhibitor with Kex2 are identical to those observed in the boro-P3−Kex2 complex. In addition, the superpositioning of the boro-P4−Kex2 structure and the structure of the CMK−furin complex shows that the different nature of the inhibitor molecules has no effect on the geometries of the bound inhibitor molecules, with the two inhibitors superpositioning quite well at P_1 (Figure 3B). Because the residues contributing to the calcium binding site and consequently to the P_1 binding site are completely conserved (Table 1) and both of these enzymes have an absolute requirement for arginine at P_1, it is not surprising that the interactions of Kex2 and furin are identical at P_1.

Interactions between Kex2 and the boro-P4 inhibitor at S_2 are again identical to that seen in the boro-P3-inhibited structure. However, both of these structures illustrate a difference between Kex2 and furin at this site (Figure 6) and more broadly, based upon the sequence alignments of Kex2 orthologues (Figure 7), seem to represent an intrinsic difference between the fungal and mammalian homologues. Whereas Kex2 has a highly negatively charged binding site with interactions between the positive charge of the ϵ-amino group of the P_2 lysine and D176, D210, and D211 (the latter through an intervening water molecule), furin has an asparagine substitution for D211 (Figures 6 and 7 and Table 1). In addition, furin and all the mammalian members of the PC family have a loop insertion between residues 185 and 192 [residues 207−211 in Kex2 (Figure 7)], which changes the positioning of D191 (D210 in Kex2) such that it is oriented away from the lysine amino group, in sharp contrast to its positioning in Kex2 (Figure 6). These changes would seem to account for the reduced importance placed upon P_2 basic residues by furin as compared to Kex2. Substitution of other residues for lysine at P_2 results in decreases in k_{cat}/K_M of approximately 100−10000-fold for Kex2 (*22*). In contrast, a similar substitution at P_2 results in an only 10-fold reduction in k_{cat}/K_M for furin (*25*). This lack of selectivity at P_2 in furin is also reflected in the minimal substrate consensus sequence for furin, which does not include a preferred P_2 residue (R-X-X-R) (*14*). On the basis of the alignment data (Figure 7), it would seem likely that all of the mammalian members of the PC family would have a selectivity similar to furin at S_2 and place a similar reduced level of importance on the necessity of basic residues at this position. In addition to the effects of these structural differences upon the substrate selectivity of the two enzymes, this slightly different S_2 pocket results in a deviation in the position of the CMK-peptidyl inhibitor in furin versus that of the peptidyl boronic acid in Kex2 that is propagated down the peptide backbone to P_4 (Figure 3B).

The structures of Kex2 and furin all show the absence of a discrete P_3 binding pocket (Figure 4). The substitution at P_3 of glutamate for alanine in the case of the boro-P4 inhibitor compared to the boro-P3-inhibited complex of Kex2 results in no change in the side chain orientation, with the glutamate carboxylate oriented away from the enzyme active site, again supporting the biochemical data that suggest that no positive selectivity occurs in Kex2 at this position (*22*).

As mentioned above, the dual specificity of Kex2 for both aliphatic and basic residues at P_4 is explained by the current structure. As mentioned previously and shown in Figure 4, there exists a hydrophobic pocket that would accommodate aliphatic residues at this position in addition to interactions that accommodate basic residues at this position. The architecture of the basic binding site at P_4, through interactions with the carboxylate of E255 and the backbone carbonyl of I250, would seem to be selective for only a terminal positive charge, and both lysine and arginine should be accommodated at P_4 in a manner similar to that for the P_2 binding site (*20*, *23*). This observation is confirmed by the kinetic data that show the substitution of arginine with citrulline at P_4 results in a reduction in k_{cat}/K_M of approximately 24-fold (Table 3 and ref *23*). Perhaps not surprisingly, due to the differences in selectivity at P_4, the Kex2 P_4 basic binding site is not the same site as used by furin, where the P_4 arginine adopts an orientation different from the one seen in Kex2. In furin, a more elaborate interaction occurs between the enzyme and arginine side chain through contacts with both the terminal positive charge and the guanidinium nitrogens (Figure 8), similar to what is observed in binding of P_1 arginine in both Kex2 and furin. This suggests that furin should be able to differentiate between lysine and arginine at P_4 and favor substrates containing a P_4 arginine residue. This is indeed what is observed in the kinetic experiments, which show a 30-fold reduction in k_{cat}/K_M for hexapeptide substrates when a substitution of arginine for lysine is made (Table 3 and ref *25*).

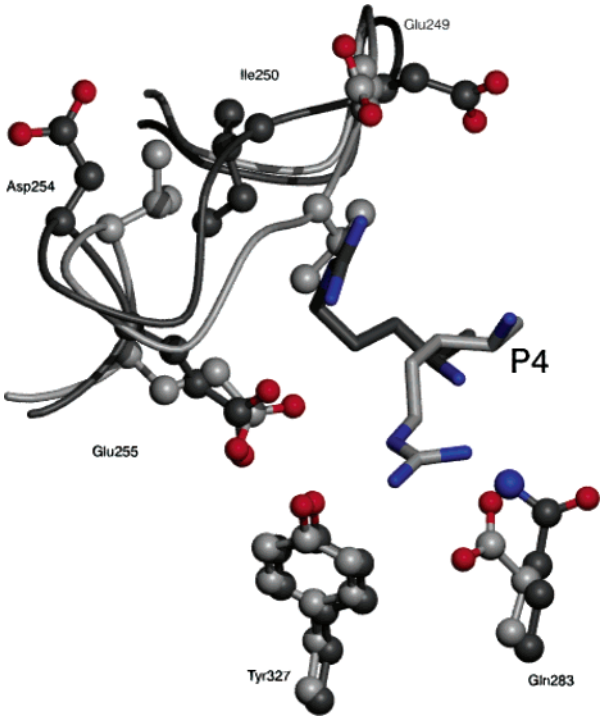

FIGURE 8: S_4 binding pockets of ssKex2 and furin. Superpositioning results of boro-P4 peptidyl boronic acid bound to ssKex2 and dec-RVKR-CMK bound to furin (PDB entry 1P8J) in the region of the S_4 binding site. Carbon atoms of the boro-P4 inhibitor are rendered in black, while the carbon atoms of the CMK bound to furin are rendered in gray. All other atoms are colored according to atom type. The amino acid side chains of ssKex2 are labeled.

This difference in binding sites at P_4 results from the repositioning of the loop from residue 249 to 252 in Kex2, such that in furin, V231 (I250 in Kex2) occupies the same location as the guanidinium group of the P_4 arginine in Kex2 (Figure 8). This precludes the binding of the P_4 arginine in furin in the same orientation as is observed in Kex2. The repositioning of this loop is dictated by the identity of the residue at position 254 in Kex2 (position 235 in furin). In Kex2, the side chain of D254 is oriented outward toward solvent, and this allows I250 to occupy a position that makes it a member of a hydrophobic pocket and stabilizing the structural element of which it is a constituent. In furin, V235 is the equivalent residue, and the side chain is oriented such that it is a member of the equivalent hydrophobic pocket. The result of this change in the orientation of the V235 side chain is the displacement of the loop (residues 249−252, Kex2) since there would be a steric clash between the side chain of V235 and V231 if the loop occupied the same orientation as in Kex2. The displacement of this loop subsequently results in the V231 side chain occupying the same space as the guanidinium group of the inhibitor side chain in Kex2, therefore steering the P_4 side chain in furin toward its binding pocket. The importance of the repositioning of the loop and subsequent preclusion of the Kex2 binding orientation in furin is supported by the mutagenic data from Kex2 that show mutation of Q283E alone is not sufficient to make a Kex2 enzyme with furin-like P_4 selectivity (L. Rozan, D. J. Krysan, N. C. Rockwell, and R. S. Fuller, manuscript in preparation). Similar to the differences exhibited at S_2, this structural difference seems to define a difference between the mammalian PC members and the fungal enzymes (Figure 7). Combined with this structural change, which precludes the Kex2 binding orientation in furin, Q283 is substituted with D264 in furin (Figures 7 and 8 and Table 1). As previously mentioned, these two alterations allow for a complex set of interactions in which E236 in furin forms a hydrogen bond with a guanidinium nitrogen of the P_4 arginine, while the short distance between the carboxyl oxygen of D236 and the hydroxyl of Y308 (2.42 Å) suggests that the tyrosine hydroxyl would be correctly ionized to hydrogen bond with one amino group of the P_4 arginine (3.2 Å). The other guanidinium amino group is thus poised to interact with the carboxylate oxygen of D264 (2.7 Å), resulting in a highly selective binding site for arginine at this position. The result of these differences is the creation of a very selective site for arginine residues at P_4 in furin that is not present in Kex2, a fact that is reflected in the kinetic data (see above) (*23*, *25*). On the basis of these observations, it should be possible to generate a Kex2 molecule with furin-like specificity at P_4 with the double mutant D254V/Q283D. In addition, exploitation of the persistent difference in substrate binding between the fungal Kex2 enzymes and the mammalian enzymes at P_4 would seem to make feasible the generation of inhibitors of Kex2 as antifungal agents that are selective for the yeast enzymes.

As a result of the different orientation adopted by the P_4 arginine in the two molecules, the N-termini of the two inhibitors can be seen to extend in different directions in the two enzyme complexes (Figure 8). The two different orientations of the termini of the inhibitor molecules could account for the differences suggested by biochemical studies for the absence of extended contacts between Kex2 and P_6-containing substrates. The N-terminus of the boro-P4 inhibitor is oriented toward Q283 (D264 in furin), which would place a putative P_5 side chain in a relatively open site adjacent to P_3 and orient the extending chain toward the cleft between the P-domain and catalytic domain identified previously (*20*). In contrast, the CMK inhibitor bound to furin extends toward E257 (A276 in Kex2), allowing P_6 residues to interact with E230 and D223 (D249 and T252, respectively, in Kex2) at the predicted S_6 pocket (*21*). In addition, the residues implicated in forming S_5 and S_6 lie in the loop (residues 249−252 in Kex2) that occupies a different conformation in each of the two enzymes, resulting in the different binding orientation of arginine at S_4. The orientation of the N-terminus of the boro-P4 inhibitor, and the lack of sequence and structural conservation in the proposed S_5 and S_6 sites, would seem to suggest that in Kex2, extended substrates would circumvent the proposed S_5 and S_6 sites of furin, providing a structural basis for the observation that while furin has extended contacts through S_6, Kex2 selectivity does not appear to extend beyond S_4. Further investigation will be needed to support this observation.

Whereas both enzymes have similar selectivity at P_4 (both recognizing basic residues), the striking difference in the way the two enzymes bind a P_4 arginine side chain provides structural evidence for the differences in the selectivity of Kex2 and furin at P_4. Moreover, this provides an explanation for differences between the two enzymes in contacts at S_5 and S_6. Exploitation of these differences may provide a structural basis for the rational design of inhibitors that are selective for the fungal Kex2 enzymes (*10*, *11*).

ACKNOWLEDGMENT

We thank Drs. Mark Wilson and Timothy Fenn for their assistance with data collection and their critical reading of the manuscript. Use of the Advanced Photon Source was supported by the U.S. Department of Energy, Basic Energy Sciences, Office of Science, under Contract W-31-109-Eng-38. Use of the BioCARS Sector 14 instrument was supported by the National Institutes of Health, National Center for Research Resources, under Grant RR07707.

REFERENCES

1. Schechter, I., and Berger, A. (1967) *Biochem. Biophys. Res. Commun. 27*, 157−162.
2. Julius, D., Brake, A., Blair, L., Kunisawa, R., and Thorner, J. (1984) *Cell 37*, 1075−1089.
3. Fuller, R. S., Brake, A. J., and Thorner, J. (1989) *Science 246*, 482−486.
4. Fuller, R. S., Brake, A., and Thorner, J. (1989) *Proc. Natl. Acad. Sci. U.S.A. 86*, 1434−1438.
5. Fuller, R. S., Sterne, R. E., and Thorner, J. (1988) *Annu. Rev. Physiol. 50*, 345−362.
6. Komano, H., and Fuller, R. S. (1995) *Proc. Natl. Acad. Sci. U.S.A. 92*, 10752−10756.
7. Martin, C., and Young, R. A. (1989) *Mol. Cell. Biol. 9*, 2341−2349.
8. Rogers, D. T., Saville, D., and Bussey, H. (1979) *Biochem. Biophys. Res. Commun. 90*, 187−193.
9. Cappellaro, C., Mrsa, V., and Tanner, W. (1998) *J. Bacteriol. 180*, 5030−5037.
10. Newport, G., Kuo, A., Flattery, A., Gill, C., Blake, J. J., Kurtz, M. B., Abruzzo, G. K., and Agabian, N. (2003) *J. Biol. Chem. 278*, 1713−1720.
11. Bader, O., Schaller, M., Klein, S., Kukula, J., Haack, K., Muhlschlegel, F., Korting, H. C., Schafer, W., and Hube, B. (2001) *Mol. Microbiol. 41*, 1431−1444.
12. Zhou, A., Webb, G., Zhu, X., and Steiner, D. F. (1999) *J. Biol. Chem. 274*, 20745−20748.
13. Smeekens, S. P. (1993) *Bio/Technology 11*, 182−186.
14. Molloy, S. S., Bresnahan, P. A., Leppla, S. H., Klimpel, K. R., and Thomas, G. (1992) *J. Biol. Chem. 267*, 16396−16402.
15. Siezen, R. J., and Leunissen, J. A. (1997) *Protein Sci. 6*, 501−523.
16. Germain, D., Dumas, F., Vernet, T., Bourbonnais, Y., Thomas, D. Y., and Boileau, G. (1992) *FEBS Lett. 299*, 283−286.
17. Wilcox, C. A., and Fuller, R. S. (1991) *J. Cell Biol. 115*, 297−307.
18. Rockwell, N. C., and Fuller, R. S. (2001) in *The Enzymes* (Dalbey, R. E., and Sigman, D. S., Eds.) pp 259, Academic Press, San Diego.
19. Gluschankof, P., and Fuller, R. S. (1994) *EMBO J. 13*, 2280−2288.
20. Holyoak, T., Wilson, M. A., Fenn, T. D., Kettner, C. A., Petsko, G. A., Fuller, R. S., and Ringe, D. (2003) *Biochemistry 42*, 6709−6718.
21. Henrich, S., Cameron, A., Bourenkov, G. P., Kiefersauer, R., Huber, R., Lindberg, I., Bode, W., and Than, M. E. (2003) *Nat. Struct. Biol. 10*, 520−526.
22. Rockwell, N. C., Wang, G. T., Krafft, G. A., and Fuller, R. S. (1997) *Biochemistry 36*, 1912−1917.
23. Rockwell, N. C., and Fuller, R. S. (1998) *Biochemistry 37*, 3386−3391.
24. Rockwell, N. C., Krysan, D. J., Komiyama, T., and Fuller, R. S. (2002) *Chem. Rev. 102*, 4525−4548.
25. Krysan, D. J., Rockwell, N. C., and Fuller, R. S. (1999) *J. Biol. Chem. 274*, 23229−23234.
26. Watanabe, T., Nakagawa, T., Ikemizu, J., Nagahama, M., Murakami, K., and Nakayama, K. (1992) *J. Biol. Chem. 267*, 8270−8274.
27. Rockwell, N. C., and Fuller, R. S. (2002) *J. Biol. Chem. 277*, 17531−17537.
28. Kettner, C., Mersinger, L., and Knabb, R. (1990) *J. Biol. Chem. 265*, 18289−18297.
29. McPherson, A. (2001) *Protein Sci. 10*, 418−422.
30. Gill, S. C., and Vonhippel, P. H. (1989) *Anal. Biochem. 182*, 319−326.
31. Holyoak, T., Fenn, T. D., Wilson, M. A., Moulin, A. G., Ringe, D., and Petsko, G. A. (2003) *Acta Crystallogr. D59*, 2356−2358.
32. Otwinowski, Z., and Minor, W. (1997) in *Methods in Enzymology* (Carter, C. W., Jr., and Sweet, R. M., Eds.) pp 307−326, Academic Press, New York.
33. Brunger, A. T., Adams, P. D., Clore, G. M., DeLano, W. L., Gros, P., Grosse-Kunstleve, R. W., Jiang, J. S., Kuszewski, J., Nilges, M., Pannu, N. S., Read, R. J., Rice, L. M., Simonson, T., and Warren, G. L. (1998) *Acta Crystallogr. D54*, 905−921.
34. Rice, L. M., and Brunger, A. T. (1994) *Proteins 19*, 277−290.
35. Brunger, A. T. (1992) *Nature 355*, 472−475.
36. Laskowski, R. A., Macarthur, M. W., Moss, D. S., and Thornton, J. M. (1993) *J. Appl. Crystallogr. 26*, 283−291.
37. Brenner, C., Bevan, A., and Fuller, R. S. (1994) *Methods Enzymol. 244*, 152−167.
38. Fenn, T. D., Ringe, D., and Petsko, G. A. (2003) *J. Appl. Crystallogr. 36*, 944−947.
39. Thompson, J. D., Higgins, D. G., and Gibson, T. J. (1994) *Nucleic Acids Res. 22*, 4673−4680.
40. Gouet, P., Courcelle, E., Stuart, D. I., and Metoz, F. (1999) *Bioinformatics 15*, 305−308.

BI035849H